Desalination and Water Treatment
www.deswater.com
doi: 10.1080/19443994.2013.798841

52 (2014) 3133–3146
April

Taylor & Francis
Taylor & Francis Group

Sorption-reduction removal of Cr(VI) from aqueous solution by the porous biomorph–genetic composite of α-Fe_2O_3/Fe_3O_4/C with eucalyptus wood hierarchical microstructure

Zongqiang Zhu[a,b], Yinian Zhu[b,*], Feng Yang[c], Xuehong Zhang[b], Hui Qin[b], Yanpeng Liang[b], Jie Liu[b]

[a]*College of Light Industry and Food Engineering, Guangxi University, Nanning, Guangxi 530004, P.R. China*
[b]*College of Environmental Science and Engineering, Guilin University of Technology, Guilin, Guangxi 541004, P.R. China*
Tel. +86 773 5891059; Fax: +86 773 5895330; email: zhuyinian@163.com
[c]*Department of Environment Engineering, Nanjing Institute of Technology, Nanjing, Jiangsu 211167, P.R. China*

Received 17 November 2012; Accepted 18 April 2013

ABSTRACT

A porous biomorph–genetic composite of α-Fe_2O_3/Fe_3O_4/C (PBGC-Fe/C) with eucalyptus wood hierarchical microstructure was prepared and characterized. The result indicated that the PBGC-Fe/C material retained the hierarchical porous structure of eucalyptus wood with three different types of pores (widths 70–120, 4.1–6.4 and 0.1–1.3 μm) originating from vessels, fibres, and pits of the wood, respectively. Batch experiments were conducted to evaluate the effects of different parameters on Cr(VI) adsorption systematically. With increasing initial concentration from 10 to 150 mg/L, the amounts of Cr(VI) adsorbed on the pulverized PBGC-Fe/C adsorbent (<0.149 mm) increased from 1.00 to 4.01 mg/g at 25 °C, from 1.00 to 4.22 mg/g at 35 °C, and from 1.00 to 4.52 mg/g at 45 °C. At the initial concentrations of 2, 10, and 50 mg/L, the adsorption capacities for the unpulverized PBGC-Fe/C adsorbent (>0.841 mm) were determined to be 0.20, 0.92, and 2.96 mg/g, respectively, which exhibited a similar average value to those of fine particles or nanoparticles of iron oxides. The adsorption followed Freundlich as well as Langmuir isotherms and could well be described by the pseudo-second-order kinetic equation. X-ray photoelectron spectroscopy studies showed that the main mechanism of Cr(VI) removal was a sorption-redox reaction between Cr(VI) and the PBGC-Fe/C adsorbent.

Keywords: Eucalyptus wood template; Biomorph-genetic magnetic composite; Iron oxide; Hierarchical porous microstructure; Sorption-redox reaction; Cr(VI)

1. Introduction

Hexavalent chromium is a well-known, highly toxic metal and is classified as the top 16th hazardous substance. The presence of high levels of chromium in the environment may cause long-term health risks to humans and ecosystems. Industrial sources of Cr(VI), include leather tanning, cooling tower blowdown, chrome plating, electroplating, anodizing baths, rinse

*Corresponding author.

waters, wood preserving, etc [1]. A wide range of treatment methods, such as adsorption, chemical precipitation, ion exchange, filtration and membrane separation, electrocoagulation, solvent extraction, reduction, and reverse osmosis have been developed for removing metal ions from water and wastewaters [2]. Most of them are very effective at removing chromium from water and wastewater containing relatively high initial chromium concentrations. Adsorption is generally known to be one of the most popular and effective techniques for chromium removal and recovery from wastewaters [3].

Metal ions are selectively adsorbed onto the adsorbent surface from wastewater with the quantity of the removed pollutant depending on the adsorption capacity of the adsorbent [4]. Various materials, such as agricultural wastes, industrial waste/by-products, zeolite, organic resins, synthesized fibers, carbon steel, lignite, peat, chars, and coals, clay minerals, and oxides/hydroxides have already been tested for their sorption efficiency of chromium from water [1]. Mineral oxides, especially Fe- and Al-oxides, are very common in the environment and have active sorption capability for metal ions [2]. Iron oxides have been, for instance, proposed for remediation of heavy metal contaminated soils due to their high removal capacity, strong binding, and low cost. Iron-based oxides are known to be good adsorbents for oxyanions removal. Magnetite is an iron oxide, which has both Fe^{2+} and Fe^{3+} species exposed on its surface. It is believed that in contact with Cr(VI) solutions, magnetite could create a surface reductive environment, where Cr(VI) could be reduced to Cr(III), remain attached to the surface, and separated as solid from the solution [5].

Generally, the iron oxides having an amorphous structure are greatly effective for removal of hazardous anions compared with crystalline structure. Recently, nanomaterials have been of considerable environmental attention due to their small particle size and large surface area [4]. Most iron oxides are fine powders that are difficult to separate from a solution [1]. Additionally, at sizes under 15 nm, magnetic separation may become ineffective and the residual nanoparticles may introduce toxicological issues in the treated water unless they are passed through nanofilters. Therefore, finding the optimal adsorbent that will enable the removal of toxic trace elements by column adsorption is an objective of many investigations. The morphology of bio-organic plant materials is characterized by a hierarchically built anatomy with microstructural features ranging from the millimeter (e.g. growth ring pattern of wood, papers) to the micrometer-scale (cellulose fibre structures) [6]. Converting biological structures into oxide/carbide-based ceramics and ceramic composites can overtake these advantages and represents an alternative ceramic manufacturing route compared with the conventional powder processing technologies and has recently become a matter of increasing interest. Cellular materials offer unique properties and the open cell materials can be useful in applications requiring interconnected porosity such as filters [6].

In the present work, the eucalyptus wood was used as microstructural templates for producing the porous biomorph–genetic composite of α-Fe_2O_3/Fe_3O_4/C (PBGC-Fe/C) and then it was characterized and used to investigate the adsorption of Cr(VI) from aqueous solution. Studies concerning the effects of initial concentration, pH, adsorbent dose, grain size, contact time, and temperature are presented and discussed. Experimental data were analyzed using kinetic equations and equilibrium isotherms, and the characteristic parameters for each model have been determined.

2. Materials and methods

2.1. Preparation of adsorbent

The generic processing route to produce the porous biomorph–genetic composite of α-Fe_2O_3/Fe_3O_4/C (PBGC-Fe/C) from eucalyptus wood template included three steps, i.e. extracting with ammonia solution, impregnating with ferric solution, and calcining.

Eucalyptus grandis wood samples from a local pulp factory were collected, air-dried, and cut into chips having the size of $30 \times 10 \times 3\,mm^3$. The rectangular specimens of eucalyptus wood were then heated in boiling 5% dilute ammonia for 6 h to remove the wood extractive compounds, e.g. gums, tropolones, fats, and fatty acids which could effectively increase the connectivity among pores and cellular. The treated templates of eucalyptus wood were washed by ultrapure water and dried at 80 °C for 24 h.

The ferric nitrate (analytically pure) was dissolved in a mixture solvent of ethanol and ultrapure water (1:1) to make a 1.2 mol/L precursor solution and then the wood templates after extraction treatment, were dipped into the precursor solution at 60 °C in covered beakers. Some precursor solution was added to keep the woods immersed always in ferric solution. After soaking for 3 days, the samples were taken out from the solution and dried in oven at 80 °C for 24 h. The above soaking–drying process was repeated three times.

Finally, the dried samples, placed in a stainless steel retort, were kept inside the muffle furnace and

heated slowly from room temperature to the predetermined carbonization temperature of 600 °C at the rate of ca. 4 °C/min. These samples were kept at their final carbonization temperature for a period of 3 h and then allowed to cool inside the furnace itself to room temperature so that the PBGC-Fe/C adsorbent was obtained.

2.2. Characterization of adsorbent

The chemical composition of the PBGC-Fe/C adsorbent was determined using Element Analyzer (EA2400II, PerkinElmer, USA). The specific surface area of the PBGC-Fe/C adsorbent was determined from nitrogen adsorption/desorption isotherms measured at −194 °C by a Quantachrome NOVAe1000. All the prepared solids before and after Cr(VI) adsorption were characterized by powder X-ray diffraction (XRD) with an X'Pert PRO diffractometer using Cu Kα radiation (40 kV and 40 mA). The morphology was analyzed by scanning electron microscopy (SEM, Jeol JSM-6380LV). At the same time, the chemical composition is assessed by the use of energy dispersive X-ray spectroscopy (EDS). The samples were also measured in the form of KBr pellets over a range of 4,000–400 cm^{-1} using a Fourier transform infrared spectrophotometer (FT-IR, Nicolet Nexus 470). X-ray photoelectron spectroscopy (XPS) analysis was employed to determine the valence state of the Cr bound on the PBGC-Fe/C adsorbent. The Cr-laden material was obtained through contact with 100 mg/L of Cr(VI) at pH 2.0 for 1 day. Prior to mounting for XPS, the PBGC-Fe/C adsorbents before and after sorption of Cr(VI) were washed with deionized-distilled water several times, and then oven-dried at 65 °C for 24 h. The spectra were collected on a VG Scientific model ESCALAB Mark II in Department of Physics, Zhejiang University. The resulting samples were transported to the spectrometer in a portable, gas-tight chamber. A consistent 2 mm spot size was analyzed on all surfaces using a Mg Kα ($h\lambda = 1253.6$ eV) X-ray source at 100 W and the spectra were recorded at 12.5 kV. The calibration of the binding energy of the spectra was performed with the C1s peak of the aliphatic carbons, which is at 284.6 eV. Analysis of the adsorbed chromium oxidation state was conducted by comparing the experimental spectra with those of the standard Cr(III) and Cr(VI).

2.3. Adsorption experiments

The stock Cr(VI) solutions were prepared with potassium dichromate ($K_2Cr_2O_7$) and nitric acid (HNO_3) of high purity grade. MilliQTM deionized water was used for all dilutions. The batch experiments were carried out in a set of plastic centrifuge tubes (100 mL) by agitating desired amounts of the unpulverized or pulverized PBGC-Fe/C adsorbent in 50 mL solutions of desired concentration and pH with an isothermal shaker (25 °C) at the agitation speed of 200 rpm for 72 h to reach equilibrium of the solid–solution mixture. After centrifuging at 4,000 rpm for 5 min, all samples were filtered through 0.45 μm micropore membrane and then the aqueous element concentrations were determined.

Three Cr(VI) concentrations (2, 10, 50 mg/L) were employed for the study of initial concentration effect on adsorption at 25 °C. Effect of adsorbent grain size was studied with different adsorbent grain sizes (>0.841 mm chip, unpulverized), 20–40 mesh (0.841–0.4 mm), 40–60 mesh (0.4–0.25 mm), 60–80 mesh (0.25–0.177 mm), 80–100 mesh (0.177–0.149 mm), and <100 mesh (<0.149 mm). The effect of pH was studied by adjusting the initial pH of Cr(VI) solutions using diluted hydrochloric acid (HCl) and sodium hydroxide (NaOH) solutions (pHs 1, 2, 3, 4, 5, 6, and 7). Nine initial Cr(VI) concentrations (10, 20, 30, 40, 50, 75, 100, 125, and 150 mg/L) with initial pH 2 were employed for the study of initial concentration effect on adsorption at 25, 35, and 45 °C. The effect of adsorbent dose was studied with ten different adsorbent doses (0.1, 0.2, 0.3, 0.4, 0.5, 0.6, 0.7, 0.8, 0.9, and 1.0 g).

Kinetic studies were carried out in a set of plastic centrifuge tubes (100 mL) at constant temperatures (25, 35, and 45 °C) by shaking 0.5 g of the PBGC-Fe/C adsorbent in 50 mL Cr(VI) solutions (2, 10, and 50 mg/L) with initial pH 2 in each capped plastic centrifuge tube at a stirring speed of 200 rpm. The aqueous samples were taken from different conical flasks at different time intervals of 5, 10, 15, 20, 30, 60, 120, 180, 240, 300, 360, 420, 480, 540, 720, 1,080, and 1440 min, respectively. Adsorption isotherms were performed in a set of plastic centrifuge tubes (100 mL) where 50 mL Cr(VI) solutions with different initial concentrations (10, 20, 30, 40, 50, 75, 100, 125, and 150 mg/L) and initial pH 2 were placed.

Aqueous Cr(VI) concentrations were determined by the 1,5-Diphenylcarbohydrazide spectrophotometric method measuring the absorbance at 540 nm by using a spectrophotometer (Lambda 25 UV/VIS, Perkin–Elmer). The total concentration of chromium was determined through absorption atomic spectrometry (Flame Atomic Adsorption Spectrophotometer, AA 700, Perkin-Elmer). The differences between the total chromium and Cr(VI) yielded the concentrations of Cr(III). The Cr(VI) removal rate (R) is calculated from: $R\ (\%) = (C_o - C_e)/C_o \times 100$, where C_o and C_e are initial and equilibrium Cr(VI) concentrations, respectively.

The amount of adsorption at time t, q_t (mg/g), was calculated as follows: $q_t = (C_o - C_t)V/W$, where C_o and C_t (mg/L) are the liquid-phase concentrations of Cr (VI) at initial and at any time t, respectively. V is the volume of the solution (L) and W is the mass of the prepared adsorbent used (g).

3. Results and discussion

3.1. Characterization of the adsorbent

The contents of C, H, and O for the porous biomorph–genetic composite of α-Fe_2O_3/Fe_3O_4/C (PBGC-Fe/C) prepared with eucalyptus wood template were determined to be 10.73–10.96%, 3.04–5.52%, and 20.46–20.52%, respectively. The iron content in the PBGC-Fe/C material was estimated to be around 62.51–65.37%.

The specific surface area of the PBGC-Fe/C adsorbent was measured to be 59.2m^2/g by BET method using N_2 adsorption isotherm at 77 K. The magnitude of the specific surface area of the unpulverized PBGC-Fe/C material prepared in this study is comparable with the data reported for naturally-occurring and synthetic iron oxide minerals [4,7,8].

The PBGC-Fe/C materials before and after adsorption of Cr(VI) were characterized using X-ray diffraction which showed the PBGC-Fe/C adsorbent consists of magnetite, hematite, and carbon (Fig. 1). The recorded diffractogram agreed perfectly in both peak position and relative intensities with the magnetite and hematite reference found in the database. The observed diffraction peaks at 29.98°, 35.37°, 43.83°, 57.48°, and 62.54° corresponded to the diffraction peaks of the reference code 01-072-2303 for magnetite (Fe_3O_4). The diffraction peaks at 24.10°, 33.11°, 35.37°, 40.79°, 49.43°, 54.00°, 57.48°, 62.54°, and 63.92° were identified as the diffraction peaks of the reference code 00-024-0072 for hematite (α-Fe_2O_3). The diffraction peaks at 42.81° and 44.62° were in agreement with the reference code 00-001-0646 for carbon (graphite).

The FT-IR spectra of the PBGC-Fe/C adsorbent are shown in Fig. 2. Infrared analysis of the PBGC-Fe/C adsorbent showed OH stretching at 3457.74 cm^{-1}, hydroxyl bending, and γ'(OH) water bending vibration or overtones of hydroxyl bending around 1631.48 cm^{-1}. Magnetite (Fe_3O_4) band appeared at 574.68 cm^{-1} and Fe–O vibration band was seen at 470.55 cm^{-1}. The bands at around 470.55–574.68 cm^{-1} and 1384.63–1459.85 cm^{-1} were attributed to Fe–O stretching vibration. Moreover, the Fe–OH bending vibration was observed at around 1027.87 cm^{-1}.

The PBGC-Fe/C material retained the hierarchical porous structure of eucalyptus wood with three different types of pores: (1) macropores (widths 70–120 μm) originating from vessels; (2) mesopores (widths 4.1–6.4 μm) originating from fibres; and (3) micropores (widths 0.1–1.3 μm) formed on the walls of the vessels giving pits (Fig. 3). It is also evident that the connectivity among different pores could be increased obviously through extracting, pre-treatment, and calcining at high temperature. Quantitative SEM–EDS peak area analysis showed Cr(VI) adsorbed the PBGC-Fe/C material up to 0.63–4.09% (w:w) (Fig. 4). The EDS spectra were collected on samples treated with a Cr(VI) concentration of 100 mg/L.

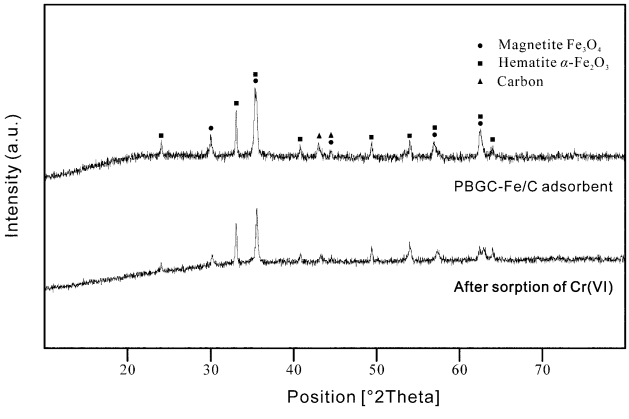

Fig. 1. XRD patterns of the PBGC-Fe/C adsorbent prepared with eucalyptus wood template.

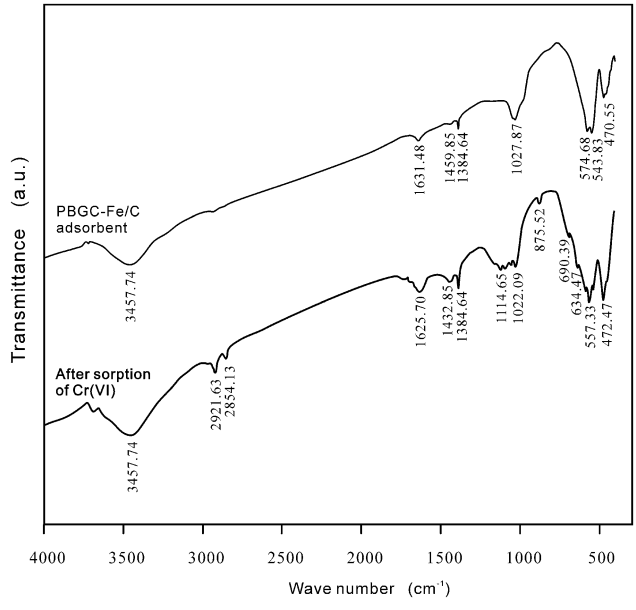

Fig. 2. FT-IR patterns of the PBGC-Fe/C adsorbent prepared with eucalyptus wood template.

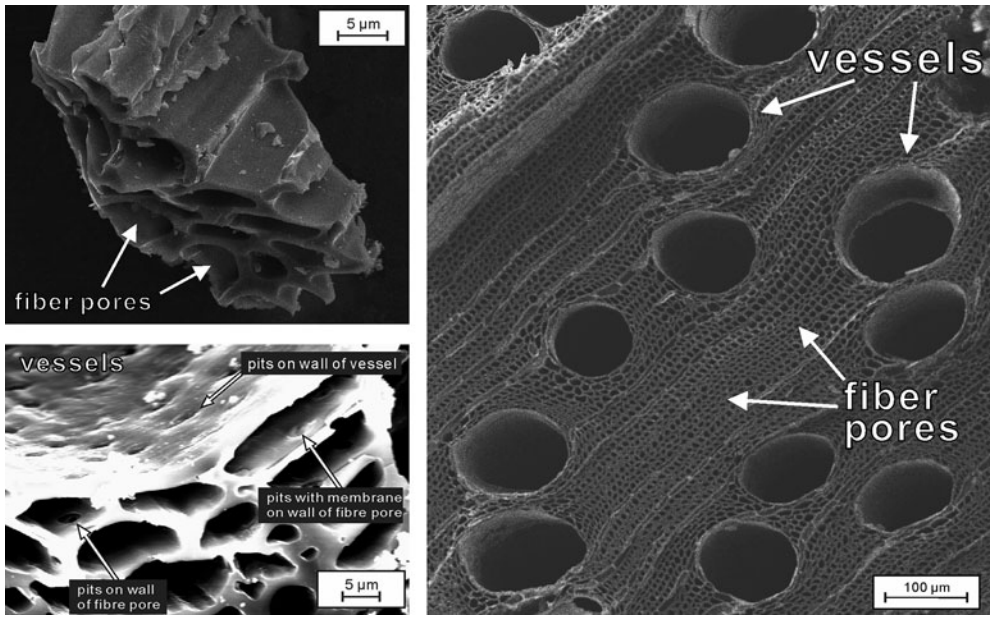

Fig. 3. SEM result of the PBGC-Fe/C adsorbent prepared with eucalyptus wood template.

3.2. Effects of adsorption conditions

3.2.1. Contact time

The Cr(VI) concentration decreased rapidly with the contact time and this confirmed strong interactions between the Cr(VI) and the adsorbent. Fig. 5 reveals that the amount of Cr(VI) adsorbed (mg/g) increased with the contact time until it gradually approached the equilibrium state. The amount of Cr(VI) adsorbed and the concentration of Cr(VI) in the liquid phase remained almost constant after adsorption for 120, 180, and 720 min at 25 °C and pH 2 with the initial Cr (VI) concentration of 2, 10, and 50 mg/L, respectively, which means that a pseudo-equilibrium of Cr(VI) adsorption was roughly attained. It is also observed that for an initial Cr(VI) concentration of 2 mg/L at 25 °C and pH 2, the maximum amount of Cr(VI) was adsorbed within the first 120 min at an average adsorption rate of 0.0017 mg/(g min) (99.36% of total

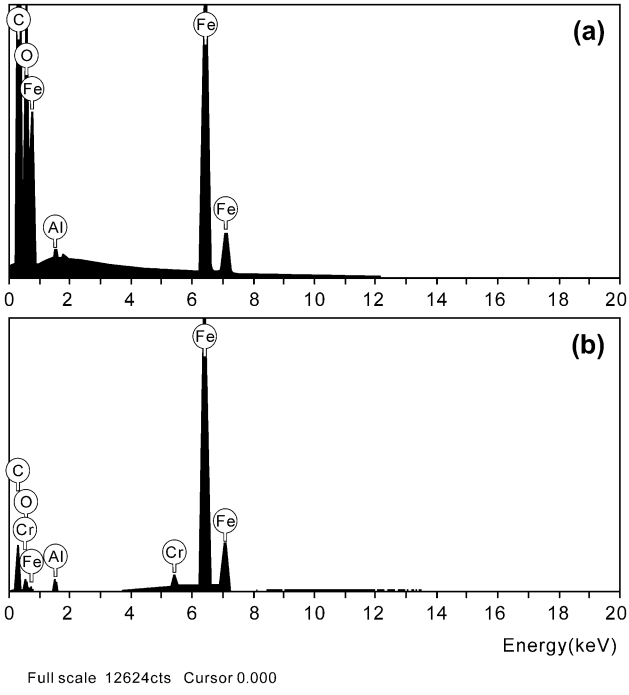

Fig. 4. SEM-EDS analysis result of the PBGC-Fe/C adsorbent prepared with eucalyptus wood template (a) before and (b) after sorption of Cr(VI).

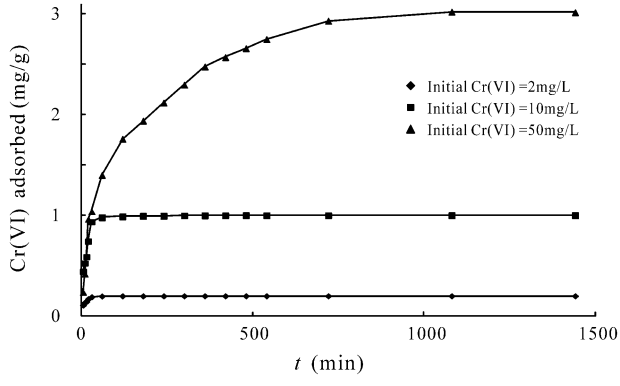

Fig. 5. Effect of contact time on Cr(VI) sorption onto the PBGC-Fe/C adsorbent (initial pH = 2; adsorbent dose 0.5 g/50 mL; 25 °C).

amount of Cr(VI) adsorbed). A similar trend was observed for the initial Cr(VI) concentrations of 10 and 50 mg/L within the first 180 and 720 min, respectively. The initial rapid uptake of adsorbate species may be due to large numbers of available vacant sites on the adsorbent surface at the initial stage.

3.2.2. Initial concentration and temperature

The initial adsorbate concentration provides an important driving force to overcome all mass transfer resistance of metal ions between the aqueous and solid phases [2]. The dependencies of the amount of Cr(VI) adsorbed and the removal percentage vs. the initial concentration are shown in Fig. 6. With increasing Cr(VI) concentrations in test solution from 10 to 150 mg/L, the actual amount of Cr(VI) adsorbed per unit mass of adsorbent increased from 1.00 to 4.01 mg/g at 25 °C, from 1.00 to 4.22 mg/g at 35 °C, and from 1.00 to 4.52 mg/g at 45 °C which confirmed strong physical and chemical interactions between Cr (VI) and the PBGC-Fe/C adsorbent. If the results are expressed in terms of percentage of Cr(VI) removed from solution, the percent adsorption decreased continuously from 99.70 to 26.71% at 25 °C, from 99.73 to 28.14% at 35 °C, and from 99.68 to 30.1% at 45 °C with increase in initial Cr(VI) concentration from 10 to 150 mg/L.

3.2.3. Initial solution pH

The amount of Cr(VI) adsorbed as a function of solution pH is shown in Fig. 7. Cr(VI) adsorption decreased as the solution pH increased, i.e. low initial pH favored the adsorption of Cr(VI) onto the PBGC-Fe/C adsorbent. At the initial Cr(VI) concentrations of 2 and 10 mg/L, most of the Cr(VI) could be adsorbed from aqueous solution and the removal rate was greater than 98%. At the initial Cr(VI) concentrations of 50 mg/L, the adsorption capacity decreased from 2.78 to 0.23 mg/g and the corresponding removal rate decreased from 55.72 to 4.63% when the initial pH increased from 1 to 7; especially, when the initial pH was greater than 3, the adsorption capacity and the corresponding removal rate decreased drastically.

The effects of pH on Cr(VI) removal are generally related to the point of zero charge (PZC) of iron oxides. The point of zero charge, pH_{PZC}, is the pH at which the surface has a net neutral charge. When the pH is lower than pH_{PZC}, the acidic water donates more protons than the surface groups and so, the adsorbent surface is positively charged (thus attracting anions). Conversely, above pH_{PZC}, the surface is negatively charged (attracting cations/repelling anions) [9]. In an acidic medium, crystalline and amorphous Fe-oxides present a potential affinity to sorb Cr(VI) [2]. The variation in removal efficiency at different pH values may be attributed to the affinities of the PBGC-Fe/C material for the different species of Cr(VI) present at different pH values. The PBGC-Fe/C material was determined to have a point of zero charge at pH_{PZC} 3.2 and can adsorb either negatively or positively charged species by electrostatic attraction depending on pH. The more acidic the condition, the more positive was the surface charge of the adsorbent and accordingly, more attractive to negative element species [8].

The pH dependence of Cr(VI) removal by magnetite and hematite could be explained by Cr(VI) speciation and the abundance of positively charged

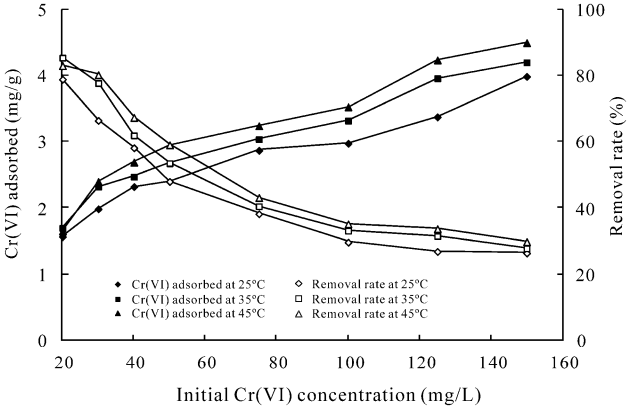

Fig. 6. Effect of initial concentration on Cr(VI) sorption onto the PBGC-Fe/C adsorbent (initial pH 2; adsorbent dose 0.5 g/50 mL; adsorbent grain size <0.149 mm).

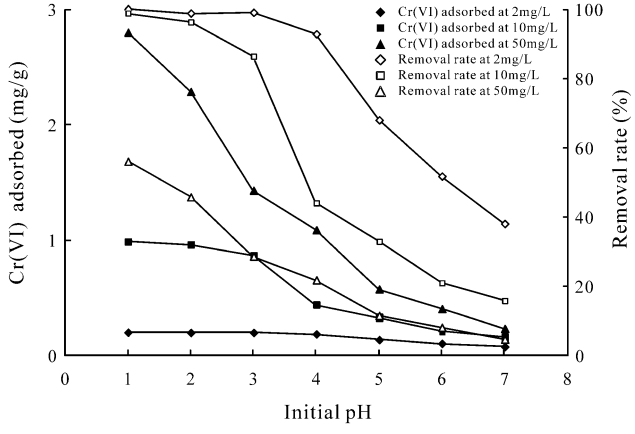

Fig. 7. Effect of initial pH on Cr(VI) sorption onto the PBGC-Fe/C adsorbent (initial concentration = 2, 10, and 50 mg/L; adsorbent dose 0.5 g/50 mL; adsorbent grain size <0.149 mm; 25 °C).

sorption sites on magnetite and hematite. The hydrolysis of Cr(VI) produces only neutral and anionic species, predominately CrO_4^{2-}, $HCrO_4^-$, $Cr_2O_7^{2-}$, and H_2CrO_4 depending on the pH. H_2CrO_4 predominates at pH levels less than about 1.0, $HCrO_4^-$ at pH levels between 1.0 and 6.0, and CrO_4^{2-} at pH levels above about 6.0. At low pH and high chromium concentrations, $Cr_2O_7^{2-}$ predominates. The best results were observed in highly acidic pH values (2.0 and sometimes 1.0) [1]. On the other hand, magnetite generates Fe^{2+} and its hydrolysis products ($FeOH^+$, $Fe(OH)_2^0$, and $Fe(OH)_3^-$) depending on the solution pH. The acidity constant of magnetite (69.2% of used adsorbent), pK_{a1} is 5.6. Thus, at pH < 5.6, dominant functional groups of iron oxide surface would be Fe^{2+} or $FeOH^+$, the iron oxide would attract negative species ($HCrO_4^-$) at low pH. At higher pH, the surface hydroxyl groups on the iron oxide surface are $Fe(OH)_2^0$ and $Fe(OH)_3^-$ and the negatively charge iron oxide surface repels negative charge species at a higher pH value [10].

3.2.4. Adsorbent dose

The amount of Cr(VI) adsorbed per unit mass of adsorbent decreased from 0.99 to 0.10 mg/g, from 2.43 to 0.50 mg/g with increasing adsorbent quantity, and from 0.1 to 1.0 g in 50 mL test solution at the initial concentration of 2 and 10 mg/L, respectively (Fig. 8). On the contrary, the corresponding percentage of Cr (VI) removed from solution increased continuously from 98.91 to 99.61% and from 48.71 to 99.93%. For the adsorption at the initial concentration of 50 mg/L, the percentage of Cr(VI) removed from aqueous solution increased continuously from 1.94 to 75.04% with increasing adsorbent mass from 0.1 to 1.0 g in 50 mL test solution, while the amount of Cr(VI) adsorbed per unit mass of adsorbent reached a maximum value of 2.68 mg/g at the adsorbent dose of 0.5 g/50 mL.

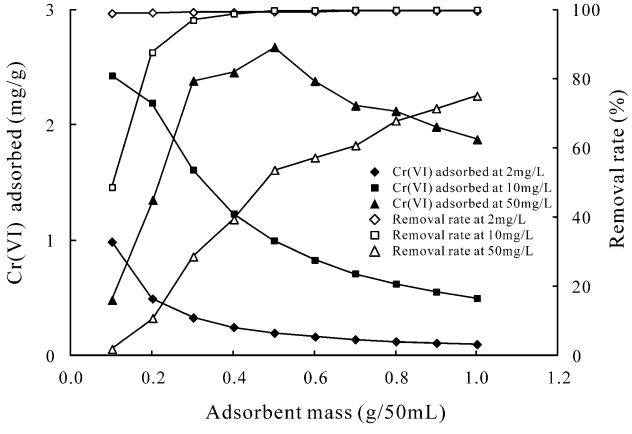

Fig. 8. Effect of adsorbent dose on Cr(VI) sorption onto the PBGC-Fe/C adsorbent (initial pH 2; initial concentration 2, 10, and 50 mg/L; adsorbent dose 0.5 g/50 mL; adsorbent grain size <0.149 mm; 25 °C).

3.2.5. Adsorbent grain size

The amounts of Cr(VI) adsorbed on the unpulverized PBGC-Fe/C sample (>20 mesh) were found to be 0.20, 0.92, and 2.96 mg/g for the adsorption at the initial Cr(VI) concentrations of 2, 10, and 50 mg/L, respectively, while the corresponding removal rates were calculated to be 99.18, 92.96, and 59.46% (Fig. 9). The results indicated that the un-pulverized PBGC-Fe/C adsorbent had a higher adsorption capacity and higher removal efficiency than the charcoal of eucalyptus wood, the sawdust of eucalyptus wood and the Fe_2O_3 powder. The adsorption capacity increased and the adsorption percentage of Cr(VI) decreased with the increase of initial concentration for all pulverized PBGC-Fe/C samples. But for the adsorption on the pulverized PBGC-Fe/C samples (<100 mesh and 100–80 mesh) at low initial Cr(VI) concentration, the effect of initial concentration on the adsorption percentage of Cr(VI) seems to be insignificant. In the case of Cr(VI) adsorption at low initial concentration, the effect of grain size on adsorption capacity and the adsorption percentage was also a little less significant. For the adsorption of Cr(VI) on the pulverized PBGC-Fe/C solids at initial concentrations of 2 and 10 mg/L, the

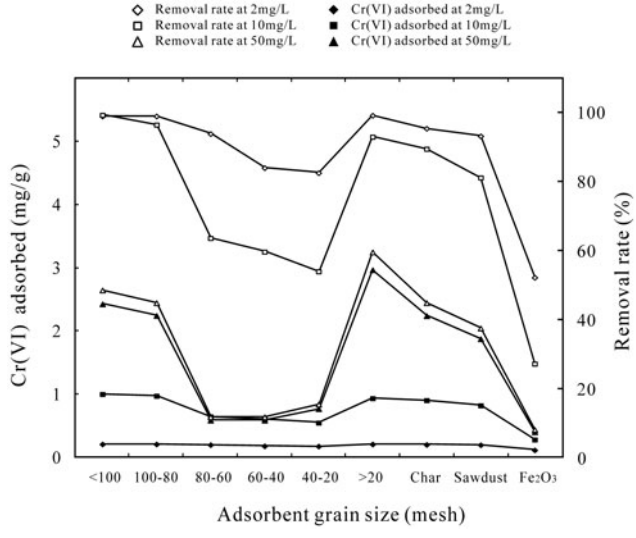

Fig. 9. Sorption of Cr(VI) by the PBGC-Fe/C adsorbent (different grain sizes), the charcoal from eucalyptus wood, the saw dust of eucalyptus wood, and the Fe_2O_3 powder (initial pH = 2; initial concentration 2, 10, and 50 mg/L; adsorbent dose 0.5 g/50 mL; 25 °C).

adsorption capacity and removal efficiency of Cr(VI) increased with the increase in the grain size. The maximum adsorption capacities and removal efficiencies were observed for the pulverized PBGC-Fe/C sample of <100 mesh (<0.149 mm) to be 0.20 mg/g and 98.98% at the initial Cr(VI) concentrations of 2 mg/L, 0.99 mg/g and 99.30% at the initial Cr(VI) concentration of 10 mg/L. In comparison with the pulverized PBGC-Fe/C sample (<100 mesh and 100–80 mesh), the unpulverized PBGC-Fe/C sample (block, >20 mesh or >0.841 mm) also had high adsorption capacities (0.20 and 0.92 mg/g) and removal efficiencies (99.18 and 92.96%) for the adsorption at the initial Cr(VI) concentrations of 2 and 10 mg/L. For the Cr(VI) adsorption on the pulverized PBGC-Fe/C sample of 80–60 mesh (0.25–0.177 mm) and 60–40 mesh (0.4–0.25 mm) at the initial Cr(VI) concentrations of 50 mg/L, the minimum adsorption capacity and removal efficiency were observed to be 0.58 mg/g and 11.54%, respectively. The highest adsorption capacity of 2.42 mg/g and the highest removal efficiency of 48.40% were found for the adsorption on the pulverized PBGC-Fe/C sample of <100 mesh (<0.149 mm). Moreover, the unpulverized PBGC-Fe/C sample (block, >0.841 mm) almost had a higher adsorption capacity and removal efficiency than the pulverized PBGC-Fe/C samples (<0.149 or 0.177–0.149 mm; <100 or 100–80 mesh).

3.3. Comparison of adsorption capacity with other iron oxide adsorbents

The adsorption capacities of the PBGC-Fe/C adsorbent for the removal of Cr(VI) have been compared with those of other adsorbents of iron oxides reported in literature [2,5,8,11–16] and the values of adsorption capacities have been presented in Table 1. Maximum adsorption capacity of Cr(VI) was determined to be 0.788 mg/g granular ferric hydroxide from a German company named Wasserchemie GmbH and Co. KG [16]. For the 20–40 nm magnetite–maghemite mixture particles obtained from Reade Advanced Materials (Rhode Island, USA, specific surface area 49 m^2/g), the maximum chromium (VI) adsorption occurred at pH 2 with values of 2.4 mg/g when the initial Cr(VI) concentration was kept at 1 mg/L [8]. The maximum adsorption capacities at pH 8 and the Cr(VI) concentrations between 0.1 and 16 mg/L were obtained for natural hematite (Johnson Matthey, purity equal to 99.999%, particle size 53 μm, specific surface area 1.7 m^2/g) and goethite (Sigma–Aldrich, purity equal to 35% Fe, particle size 10 μm, surface area 11.6 m^2/g) were 2.299 and 1.955 mg/g, respectively [2]. The amount of the adsorbed Cr(VI) on natural magnetite (particle size 0.389–0.5 mm) was 0.43 mg/g at pH 3 and the initial Cr(VI) concentration was 10 mg/L [11]. At the initial concentrations of 2, 10, and 50 mg/L, the adsorption capacities for the unpulverized PBGC-Fe/C adsorbent (>0.841 mm) were determined to be 0.20, 0.92, and 2.96 mg/g, respectively, which exhibited a similar average value for those of fine particles or nanoparticles of iron oxides reported in the literatures.

3.4. Adsorption kinetics

Kinetics of Cr(VI) adsorption onto the PBGC-Fe/C adsorbent followed the pseudo-second -order model (Fig. 10). Based on equilibrium adsorption, the equation corresponding to the pseudo-second-order kinetic model is expressed as following [17]:

$$\frac{t}{q_t} = \frac{1}{k_2 q_e^2} + \frac{t}{q_e} \quad (1)$$

The initial sorption rate, h (mg/(g min)) can be expressed:

$$h = k_2 q_e^2 \quad (2)$$

where the initial adsorption rate (h), the equilibrium adsorption capacity (q_e), and the second-order constants k_2 (g/(mg min)) can be determined experimentally from the slope and intercept of plot t/q_t vs. t (Fig. 10). The calculated correlations are closer to unity for second-order kinetics model ($R^2 = 0.9968$–1.0000); therefore, the adsorption kinetics could well be approximated more favorably by second-order-kinetic model for Cr(VI) adsorption onto the PBGC-Fe/C adsorbent. The k_2 and h values calculated from Fig. 10 are 0.0038–2.1156 g/(mg min) and 0.0382–0.2383 mg/(g min), respectively (Table 2).

3.5. Adsorption isotherm

Adsorption equilibrium measurements are used to determine the maximum or ultimate adsorption capacity. Many types of adsorption isotherms exist in literature but Freundlich and Langmuir isotherms are the two-well established equilibrium models that are most commonly used.

3.5.1. Langmuir isotherm

The Langmuir model is valid for monolayer sorption a surface with a finite number of similar active sites [18]. Langmuir isotherm is represented by the following equation:

Table 1
Comparison of results obtained in this study for the removal of Cr(VI) with those of iron oxides and their adsorption capacities in literature

Adsorbent	pH	Concentr. (mg/L)	Surface area (m^2/g)	Grain size (mm)	T (°C)	Method	Capacity (mg/g)	Ref.
PBGC-Fe/C	2–3	2	59.2	>0.841	25	–	0.20	This study
PBGC-Fe/C	2–3	10	59.2	>0.841	25	–	0.92	This study
PBGC-Fe/C	2–3	50	59.2	>0.841	25	–	2.96	This study
PBGC-Fe/C	2	10–150	–	<0.149	25	Langmuir	3.87	This study
PBGC-Fe/C	2	10–150	–	<0.149	35	Langmuir	4.21	This study
PBGC-Fe/C	2	10–150	–	<0.149	45	Langmuir	4.52	This study
α-Fe_2O_3	2–3	2	–	<0.25	25	–	0.10	This study
α-Fe_2O_3	2–3	10	–	<0.25	25	–	0.27	This study
α-Fe_2O_3	2–3	50	–	<0.25	25	–	0.39	This study
Magnetite	3	10	–	0.389–0.5	25	–	0.43	[11]
Magnetite	5.5	5	2.366	0.074–0.149	25	–	0.04	[11]
Magnetite	Neutral	5	4.29	<0.074	25	–	0.20	[12]
Magnetite	3.5	20–200	84	10–40 nm	Room	Freundlich	25	[5]
Magnetite	2	20–180	–	30–30 nm	20	Langmuir	10.50	[13]
Magnetite	2	50–500	–	100 nm	25	Langmuir	78.13	[14]
Magnetite	2	10–200	–	40–300 nm	22.5	Freundlich	41.00	[15]
Hematite	3	10	–	0.389–0.5	25	–	0.63	[11]
Hematite	5.5	5	3.285	0.074–0.149	25	–	0.43	[11]
Hematite	8	0.1–16	1.7	0.053	Room	Langmuir	2.299	[2]
Goethite	8	0.1–16	11.6	0.01	Room	Langmuir	1.955	[2]
Granular ferric hydroxide	7	0.25–3	280	0.32–2	25	Freundlich	0.788	[16]

$$C_e/q_e = 1/(q_m \times K_L) + C_e/q_m \quad (3)$$

$$R_L = 1/(1 + K_L C_o) \quad (4)$$

where C_e is the concentration of Cr(VI) solution (mg/L) at equilibrium. The constant q_m signifies the adsorption capacity (mg/g) and K_L is Langmuir constant related to the free energy of adsorption (L/mg). Linear plot of C_e/q_e vs. C_e shows that the Langmuir isotherm could yield good fits for Cr(VI) adsorption onto the PBGC-Fe/C adsorbent with R^2 values of 0.9640, 0.9720, and 0.9739 for the adsorption at 25, 35, and 45 °C, respectively (Fig. 11). Values of q_m and K_L were calculated from the slope and intercept of the linear plot and are presented in Table 2.

The essential features of Langmuir adsorption isotherm can be expressed in terms of a dimensionless constant called the separation factor or equilibrium parameter (R_L), defined by the following equation:

where K_L is the Langmuir adsorption constant and C_o is the initial Cr(VI) concentration (mg/L). R_L values indicate the type of isotherms to be either unfavorable ($R_L > 1$), linear ($R_L = 1$), favorable ($0 < R_L < 1$), or irreversible ($R_L < 0$). Table 2 also shows that the R_L values of 0.0479–0.4914 near zero confirmed the favorable uptake of Cr(VI).

The changes in free energy, enthalpy, and entropy of adsorption can be calculated from the Langmuir constant K_L. The negative values of the calculated ΔG^o (−4.1024, −4.7285, and −5.0246 kJ/mol) indicated the spontaneous nature of adsorption for Cr(VI) at 25, 35, and 45 °C and confirmed affinity of sorbent for Cr (VI). The positive calculated values of ΔH° (9.3591 J/mol) showed the endothermic nature of adsorption.

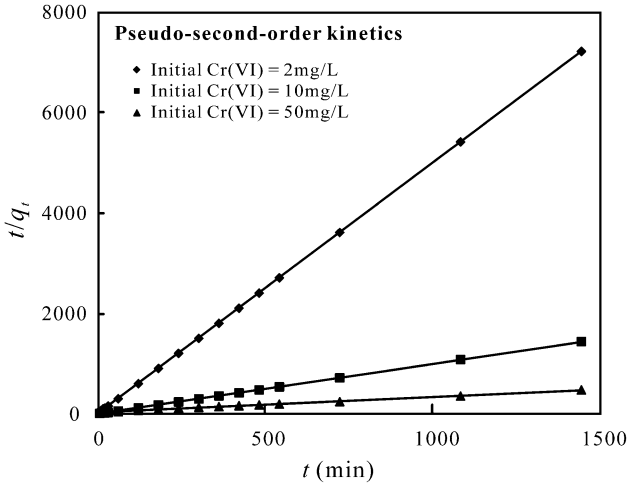

Fig. 10. Kinetics for Cr(VI) sorption onto the PBGC-Fe/C adsorbent (initial pH = 2; adsorbent dose 0.5 g/50 mL; adsorbent grain size <0.149 mm; 25 °C).

The positive values of ΔS° (0.0461 kJ/(mol K)) suggested the increased randomness at the solid/solution interface during the adsorption of Cr(VI) on the adsorbent [19].

3.5.2. Freundlich isotherm

The Freundlich isotherm can be used for nonideal sorption that involves heterogeneous surface energy systems and is expressed by the following equation:

$$\ln q_e = \ln K_F + 1/n \ln C_e \quad (5)$$

where Freundlich constant K_F ($mg^{1-1/n} L^{1/n} g^{-1}$) is a rough indicator of the adsorption capacity and $1/n$ is the adsorption intensity. The values of K_F and $1/n$ were calculated from the intercept and slope of plots (Fig. 11, Table 2). The correlation coefficients (R^2) were found to be 0.9174, 0.9553, and 0.9478 for the adsorption at 25, 35, and 45 °C, respectively, which indicated that the Freundlich isotherm gave a good fit. $1/n$ is the heterogeneity factor and can be used as a measure of the deviation from linearity of the adsorption. In this study, $1/n$ values were calculated from the slope of plots to be 0.1602–0.1857 which ranged between 0 and 1 and implied that the adsorption process was chemical. All the Cr(VI) adsorption data obtained fitted well to both Langmuir and Freundlich models, however, the calculated correlation coefficients for the Langmuir isotherm model were a little higher than those for the Freundlich (Table 2). Therefore, the Langmuir isotherm yielded a better fit to the experimental data.

3.6. Adsorption mechanisms

The mechanism by which Cr(VI) ions were adsorbed onto maghemite nanoparticles was examined using laboratory experiments and spectroscopic techniques. For testing whether any chemical redox reaction occurred during the adsorption process, it is necessary to perform the analysis of chromium contents in the solution and the particle surface [20]. From the analytical results s, the concentration of Cr(VI) always equaled that of total Cr, i.e. chromium valence in solution never changed after the adsorption process.

Table 2
Kinetic and isotherm parameters for the Cr(VI) sorption onto the PBGC-Fe/C adsorbent

Initial Cr(VI) concentration (mg/L)	k_2 (g/(mg min))	h (g/(mg min))	q_e (mg/g)	R^2
Pseudo-second-order constants				
2	2.1165	0.0846	0.1999	1.0000
10	0.2365	0.2383	1.0037	1.0000
50	0.0038	0.0382	3.1827	0.9968
Langmuir constants				
Temperature (°C)	q_m (mg/g)	K_L (L/mg)	R_L	R^2
25	3.87	0.1035	0.0605–0.4914	0.9640
35	4.21	0.1255	0.0504–0.4434	0.9720
45	4.52	0.1325	0.0479–0.4302	0.9739
Freundlich constants				
Temperature (°C)	K_F ($mg^{1-1/n} L^{1/n} g^{-1}$)	$1/n$		R^2
25	1.5383	0.1602		0.9174
35	1.6793	0.1693		0.9553
45	1.7011	0.1857		0.9478

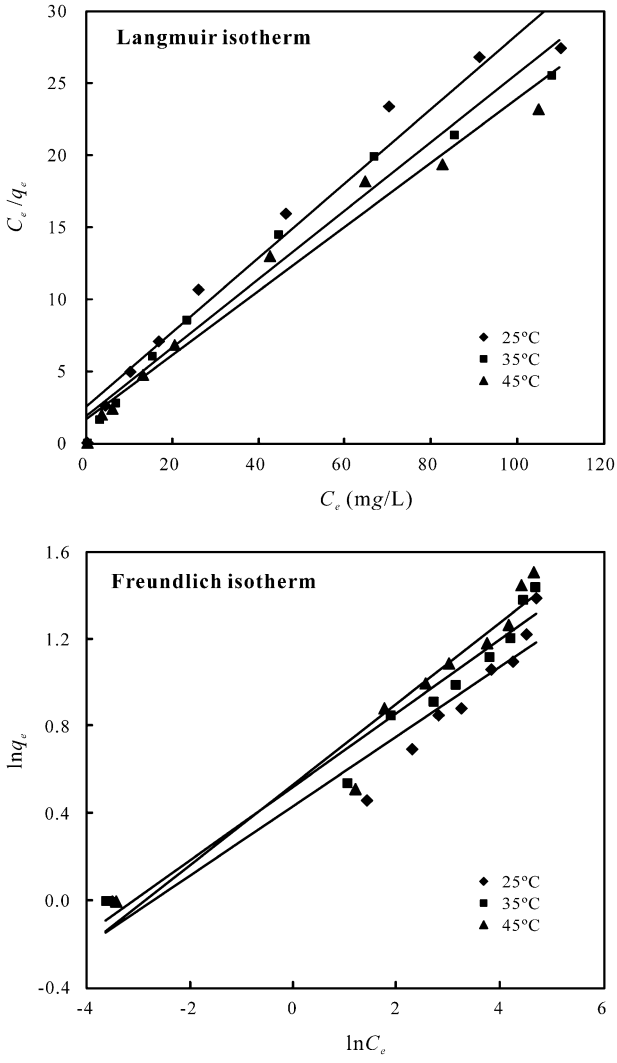

Fig. 11. Isotherm for Cr(VI) sorption onto the PBGC-Fe/C adsorbent (initial pH = 2; adsorbent dose 0.5 g/50 mL; adsorbent grain size <0.149 mm).

The Cr-loaded PBGC-Fe/C particles were also characterized by XRD, FT-IR, SEM-EDS, and XPS techniques. The results from XRD (Fig. 1) show that the identical peaks of the PBGC-Fe/C materials before and after adsorption of Cr(VI) matched well with each other. No evidence of secondary mineral precipitation was observed in the dissolution experiment, i.e. without other crystalline phases appearing after adsorption. The FT-IR spectrum corresponding to the PBGC-Fe/C adsorbent loaded with Cr(VI) exhibits some apparent shifts in the band absorption peaks of 1631.48, 1027.87, and 574.68 cm^{-1} with few changes in other bands (Fig. 2). These results indicate that magnetite (Fe_3O_4) and the hydroxyl groups specifically play a major role in Cr(VI) sorption and binding onto the surface of the PBGC-Fe/C adsorbent. In the FT-IR spectra of the PBGC-Fe/C adsorbent after adsorption of Cr(VI), the characteristic bands of CrO_4^{2-} were slightly observed at 875.52 and 557.33 cm^{-1} which can be assigned to the absorptions of Cr=O and Cr–O–Cr groups. The EDS spectrum gave the characteristic peaks for Cr(VI) at 0.50 and 5.42 keV that confirmed the binding of the Cr(VI) ions to the PBGC-Fe/C surface (Fig. 4).

Fig. 12 presents the XPS wide scan of the PBGC-Fe/C adsorbent before and after adsorption of Cr(VI) at the initial concentration of 100 mg/L. The photoelectron peaks reveal that the surface of the PBGC-Fe/C adsorbent consisted mainly of carbon (279.5 eV, C 1s), oxygen (526.5 eV, O 1s), and iron (708 eV and 720.5 eV Fe 2p). A detailed XPS survey on the C 1s, O 1s, Fe 2p, and Cr 2p regions for the PBGC-Fe/C adsorbent before and after the adsorption of Cr(VI) is also presented in the figure.

The XPS spectrum of the detailed survey on the Cr 2p region displays Cr 2p peaks (Fig. 12). Two Cr 2p3/2 peaks in the spectrum of the PBGC-Fe/C adsorbent loaded with Cr(VI) are located at 573.8 and 580.0 eV, which are close to the binding energy of the references in Cr(III) and Cr(VI), respectively. Cr(VI) was characterized by higher binding energies than Cr(III) since the hexavalent form draws electrons more strongly than the trivalent form [21]. The results indicate that Cr(III) and Fe(III) were the dominant species on the surface of magnetite after reaction. Therefore, Cr(III) was present on the surface of the PBGC-Fe/C adsorbent when it was immersed in Cr(VI). This implies that the adsorption process involved the reductive transformation of Cr(VI) into Cr(III) on the contact surface. The intensity of the Cr(III) 2p3/2 peak was obviously higher than that of the Cr(VI) 2p3/2 peak which suggested that most of Cr(VI) anions were reduced to Cr(III) during the sorption in the kinetics of the Cr(VI) + 3Fe(II) = Cr(III) + 3Fe(III) redox reaction [22]. Cr(VI) peaks were observed on the surface of magnetite indicating that the magnetite surface was oversaturated by Cr(VI), and Cr(VI) adsorbed could not be fully reduced. In contrast, the Cr(VI) peak was negligible on the surface as the reductive capacity increased [23]. Moreover, no Cr(III) was detected in the aqueous solution after the PBGC-Fe/C materials were immersed in Cr(VI) solutions which indicated that Cr(III) was not obviously released into the solution during the sorption-redox process under the present experimental conditions.

The chemical forms of the different elements can be determined according to their binding energies. The single peak and binding energies suggest that C mainly exist in the form of OC functional groups [24]. The XPS spectrum of the detailed survey on the C 1s

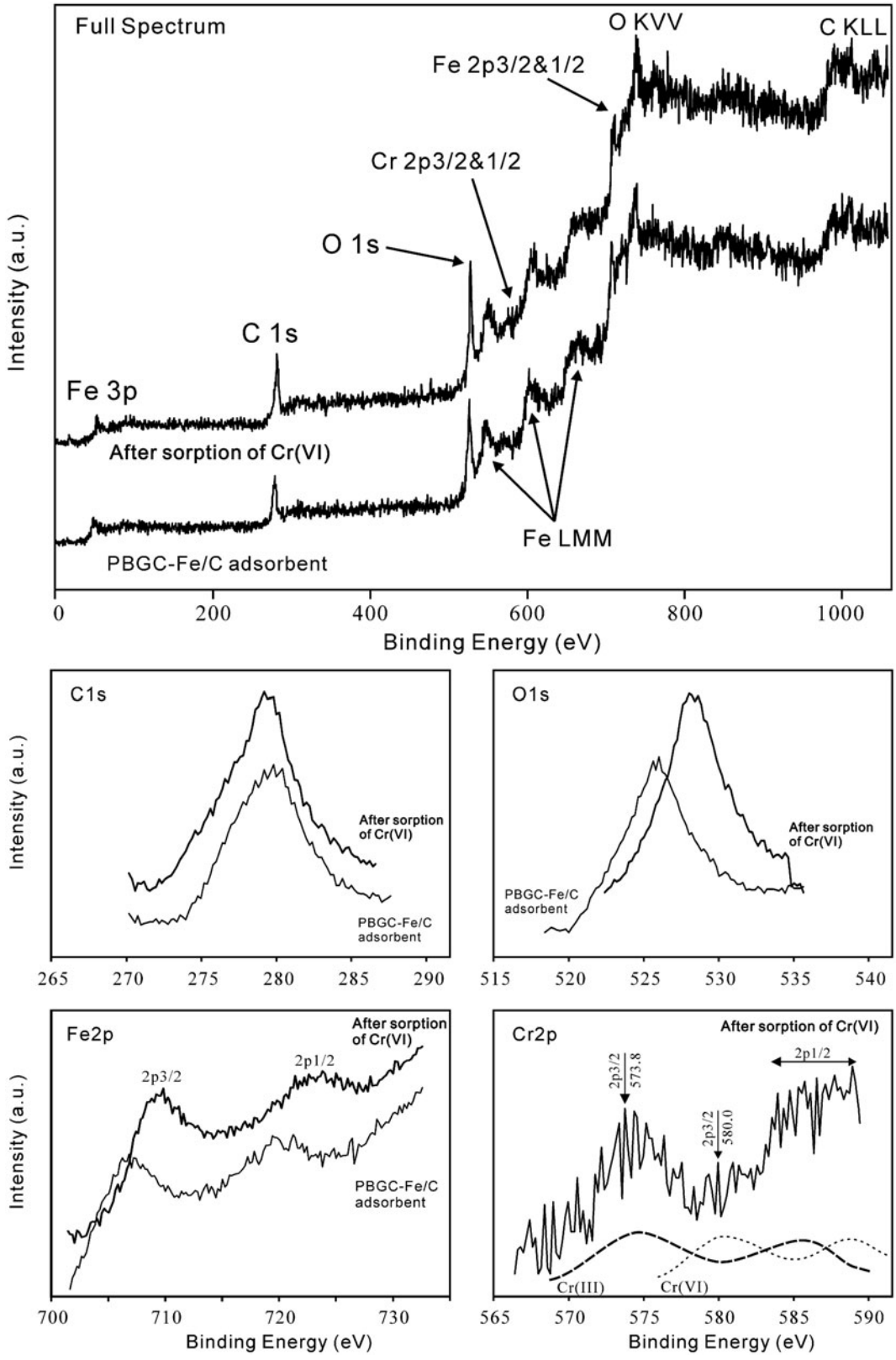

Fig. 12. XPS spectra of the PBGC-Fe/C adsorbent prepared with eucalyptus wood template before and after sorption of Cr(VI).

region showed that the C 1s peaks in the spectrum of the PBGC-Fe/C adsorbent before and after sorption of Cr(VI) are located at 279.8 and 279.2 eV, respectively. The OC functional groups can adsorb Cr(VI) but cannot supply electron charge; the OC groups have no reducing capacity for Cr(VI) [24].

Fig. 12 demonstrates that the peaks of O and Fe shift in the XPS spectra. A fundamental relation between XPS shifts and charge is available for oxygen in the following formula [24]:

$$Q = -4.372 + \{[385.023 - 8.976 \times (545.509 - E_B)]^{1/2}\}/4.488 \quad (6)$$

where Q is the average oxygen charge (esu) and E_B is the experimental value of binding energy (eV). As illustrated in Fig. 12, the binding energy of O 1s spectrum exhibits obvious change from 526.0 to 528.0 eV after Cr(VI) adsorption. The average oxygen charges at these two values are −1.144 and −1.009, respectively, indicating that the binding energy of the inner electron of O1s has a notable variation. The binding energies of the peaks in Fig. 12 are located at 526.0 and 528.0 eV representing metal–oxide (Fe–O) bonds in solution at pH 2. This suggests that Fe–O functional groups can not only adsorb Cr(VI) but can also supply the electron charge. Thus, the Fe–O groups have the reducing capacity for Cr(VI).

The binding energy of the typical XPS spectra of Fe 2p3/2 and Fe 2p1/2 exhibits a significant change from 706.8 to 709.8 eV and 721.2 to 723.8 eV after sorption of Cr(VI), respectively. For the PBGC-Fe/C material after sorption of Cr(VI), the value of 709.8 eV for the main Fe 2p3/2 peak falls within the range of values (708.2–711.3 eV) reported for goethite and other Fe(III) species such as Fe_2O_3 [25]. The position of the peak (706.8 eV) from the PBGC-Fe/C material before sorption of Cr(VI) is consistent with reduced iron species, although it lies to lower binding energy than the corresponding peak for FeO (∼709.6 eV) [25]. This indicates that Fe(III) is dominant on the surfaces of magnetite suggesting that Fe(II) on the magnetite surfaces was transformed to Fe(III) by the oxidation with Cr(VI) [23]. This suggests that the Fe(II) electron binding energy of the inner layer of electrons increases. Fe(II) has an obvious tendency to lose electrons, making it positively charged. The negative charge on the surface of Fe(II) moves from the inner layer of the adsorbent to their outer shell. The Fe(II)-containing electron-donor groups exhibit a loss of electrons in the process of Cr(VI) reduction; the Fe(II) O-groups served as electron-donor groups in the process of reduction–sorption. Additionally, the Fe 2p3/2 and Fe 2p1/2 binding energies of the Cr(VI)-sorbed PBGC-Fe/C material were higher than those of the original PBGC-Fe/C material. The increase in the binding energy of Fe 2p1/2 was previously suggested as an indication of the substitution of Cr(III) for Fe (III) in Cr-substituted magnetites [26,27] so, possibly, the isomorphic substitution of Fe(III) by Cr(III) took place in the PBGC-Fe/C material considering that Fe (III) and Cr(III) have similar ionic radii (0.067 nm for Fe(III) and 0.065 nm for Cr(III)) and the substitution of Cr(III) for Fe(III) is thermodynamically favored [26,27]. In a neutral or alkalic medium, Cr(VI) adsorbed on the surfaces of magnetite can be reductively transformed to Cr(III) and form Cr(III) (oxy) hydroxides and/or $Fe_xCr_{(1-x)}(OH)_3$ on the surface. The metal (oxy)hydroxides seem to overlay the oxidized magnetite surfaces, mainly composed of Fe(III) oxides, during the reaction [23].

4. Conclusions

The PBGC-Fe/C material retained the hierarchical porous structure of eucalyptus wood with three different types of pores (widths 70–120 μm, 4.1–6.4 μm, and 0.1–1.3 μm) originating from vessels, fibres, and pits, respectively. Its surface area was measured to be 59.2 m^2/g that is comparable with the data reported for naturally-occurring and synthetic iron oxide minerals.

The PBGC-Fe/C adsorbent could effectively remove Cr(VI) ions from the aqueous solution. By increasing initial Cr(VI) concentration from 10 to 150 mg/L, the amounts of Cr(VI) adsorbed on the pulverized PBGC-Fe/C adsorbent (<0.149 mm) increased from 1.00 to 4.01 mg/g at 25 °C, from 1.00 to 4.22 mg/g at 35 °C, and from 1.00 to 4.52 mg/g at 45 °C and the corresponding removal rates decreased from 99.70 to 26.71% at 25 °C, from 99.73 to 28.14% at 35 °C, and from 99.68 to 30.1% at 45 °C. The low pH favored Cr (VI) adsorption. At the initial concentrations of 2, 10, and 50 mg/L, the adsorption capacities for the unpulverized PBGC-Fe/C adsorbent (>0.841 mm) were determined to be 0.20, 0.92, and 2.96 mg/g, respectively, while the corresponding removal rates were calculated to be 99.18, 92.96, and 59.46% which exhibited a similar average value to those of fine particles or nanoparticles of iron oxides reported in the literatures.

The pseudo-second-order equation generated the best fit to the experimental data with regression coefficients, $R^2 > 0.9968$. The equilibrium data were found to fit both Freundlich and Langmuir isotherm equations. XPS studies showed that most of the Cr bound on the PBGC-Fe/C adsorbent was in trivalent form. The reaction mechanism on the surface of the PBGC-Fe/C material was the adsorption of Cr(VI) followed by

reductive transformation into Cr(III) on the reactive surfaces. The PBGC-Fe/C adsorbent has a potential application in the conversion of toxic Cr(VI) into less toxic or nontoxic Cr(III).

Acknowledgments

The manuscript has greatly benefited from insightful comments by anonymous reviewers. The authors thank the Guangxi Key Laboratory of Environmental Pollution Control Theory and Technology for the research assistance and the financial supports from the National Natural Science Foundation of China (NSFC40773059, NSFC41263009), the Guangxi Science and Technology Development Project (GuiKeZhong1298002-3), the Provincial Natural Science Foundation of of Guangxi (2012GXNSFDA053022, 2011GXNSFF018003).

References

[1] D. Mohan, C.U. Pittman, Activated carbons and low cost adsorbents for remediation of tri- and hexavalent chromium from water, J. Hazard. Mater. B 137 (2006) 762–811.
[2] O. Ajouyed, C. Hurel, M. Ammari, L.L. Ben Allal, N. Marmier, Sorption of Cr(VI) onto natural iron and aluminum (oxy) hydroxides: Effects of pH, ionic strength and initial concentration, J. Hazard. Mater. 174 (2010) 616–622.
[3] W. Kuang, Y. Tan, L. Fu, Adsorption kinetics and adsorption isotherm studies of chromium from aqueous solutions by HPAM-chitosan gel beads, Desalin. Water Treat. 45 (2012) 222–228.
[4] S. Yean, L. Cong, C.T. Yavuz, J.T. Mayo, W.W. Yu, A.T. Kan, V.L. Colvin, M.B. Tomson, Effect of magnetite particle size on adsorption and desorption of arsenite and arsenate, J. Mater. Res. 20 (2005) 3255–3264.
[5] G.P. Gallios, M. Vaclavikova, Removal of chromium (VI) from water streams: A thermodynamic study, Environ. Chem. Lett. 6 (2008) 235–240.
[6] H. Sieber, Biomimetic synthesis of ceramics and ceramic composites, Mater. Sci. Eng. A 412 (2005) 43–47.
[7] C. Su, R.W. Puls, Arsenate and arsenite sorption on magnetite: Relations to groundwater arsenic treatment using zerovalent iron and natural attenuation, Water Air Soil Pollut. 193 (2008) 65–78.
[8] S.R. Chowdhury, E.K. Yanful, Arsenic and chromium removal by mixed magnetite-maghemite nanoparticles and the effect of phosphate on removal, J. Environ. Manage. 91 (2010) 2238–2247.
[9] G. Muñiz, V. Fierro, A. Celzard, G. Furdin, G. Gonzalez-Sánchez, M.L. Ballinas, Synthesis, characterization and performance in arsenic removal of iron-doped activated carbons prepared by impregnation with Fe(III) and Fe(II), J. Hazard. Mater. 165 (2009) 893–902.
[10] R.M. Cornell, U. Schwertmann, The Iron Oxides: Structure, Properties, Reactions, Occurrences, and Uses, second ed., Wiley-VCH, Weinheim, 2003.
[11] Q. Wang, Cr(VI) removal in aqueous solution by iron ore and bacteria synergistic reaction, Doctor degree thesis, Zhejiang University, Hangzhou, October 2010.
[12] J. Zhao, Experimental treatment of Hg(II) and Cd(II) and Cr (VI) bearing in wastewater by natural magnetite and limonite, Master degree thesis, China University of Geosciences, Beijing, April 2002.
[13] N. Javadi, S.H. Raygan, S.A. Seyyed Ebrahimi, Production of nanocrystalline magnetite for adsorption of Cr(VI) ions, Int. J. Mod. Phys. A 5 (2012) 771–783.
[14] Y. Pang, G. Zeng, L. Tang, Y. Zhang, Y. Liu, X. Lei, Z. Li, J. Zhang, Z. Liu, Y. Xiong, Preparation and application of stability enhanced magnetic nanoparticles for rapid removal of Cr(VI), Chem. Eng. J. 175 (2011) 222–227.
[15] M.M. Amin, A. Khodabakhshi, M. Mozafari, B. Bina, S. Kheiri, Removal of Cr(VI) from simulated electroplating wastewater by magnetite nanoparticles, Environ. Eng. Manage. J. 9 (2010) 921–927.
[16] A.R. Asgari, F. Vaezi, S. Nasseri, O. Dördelmann, A.H. Mahvi, E. Dehghani Fard, Removal of hexavalent chromium from drinking water by granular ferric hydroxide, Iran. J. Environ. Health 5 (2008) 277–282.
[17] Y.S. Ho, G. McKay, Pseudo-second order model for sorption processes, Process Biochem. 34 (1999) 451–465.
[18] D.Q.L. Oliveira, M. Gonçalves, L.C.A. Oliveira, L.R.G. Guilherme, Removal of As(V) and Cr(VI) from aqueous solutions using solid waste from leather industry, J. Hazard. Mater. 151 (2008) 280–284.
[19] S. Wang, Z.H. Zhu, Effects of acidic treatment of activated carbons on dye adsorption, Dyes Pigm. 75 (2007) 306–314.
[20] J. Hu, G. Chen, I.M.C. Lo, Removal and recovery of Cr(VI) from wastewater by maghemite nanoparticles, Water Res. 39 (2005) 4528–4536.
[21] D. Park, S.R. Lim, Y.S. Yun, J.M. Park, Reliable evidences that the removal mechanism of hexavalent chromium by natural biomaterials is adsorption-coupled reduction, Chemosphere 70 (2007) 298–305.
[22] T. Kendelewicz, P. Liu, C.S. Doyle, G.E. Brown, E.J. Nelson, S.A. Chambers, X-ray absorption and photoemission study of the adsorption of aqueous Cr(VI) on single crystal hematite and magnetite surfaces, Surf. Sci. 424 (1999) 219–231.
[23] Y. Jung, J. Choi, W. Lee, Spectroscopic investigation of magnetite surface for the reduction of hexavalent chromium, Chemosphere 68 (2007) 1968–1975.
[24] J. Li, Q. Lina, X. Zhang, Mechanism of electron transfer in the bioadsorption of hexavalent chromium within *Leersia hexandra* Swartz granules by X-ray photoelectron spectroscopy, J. Hazard. Mater. 182 (2010) 598–602.
[25] H. Abdel-Samad, P.R. Watson, An XPS study of the adsorption of chromate on goethite (α-FeOOH), Appl. Surf. Sci. 108 (1997) 371–377.
[26] J. Manjanna, G. Venkateswaran, Effect of oxidative pretreatment for the dissolution of Cr-substituted hematites/magnetites, Ind. Eng. Chem. Res. 41 (2002) 3053–3063.
[27] P. Yuan, D. Liu, M. Fan, D. Yang, R. Zhu, F. Ge, J. Zhu, H. He, Removal of hexavalent chromium [Cr(VI)] from aqueous solutions by the diatomite-supported/unsupported magnetite nanoparticles, J. Hazard. Mater. 173 (2010) 614–621.